PREDICTION OF LAMINAR-TO-TURBULENT TRANSITION IN INCOMPRESSIBLE FLOW PAST 3-D CAVITY

H. Yao, R. K. Cooper, E. Benard, and S. Raghunathan
School of Aeronautical Engineering
Queen's University Belfast, Belfast BT7 1NN, UK

Keywords: *laminar-to-turbulent transition, incompressible flow, 3-D cavity*

Abstract

This paper investigates laminar-to-turbulent transition in incompressible flow past a 3-D open shallow rectangular cavity. Previous studies have indicated that the transition may occur at high Reynolds numbers. This study includes two parts: 1) numerical simulation of the transition, and 2) prediction of the area of the transition in the shear layer of the cavity. The large eddy simulation (LES) approach is used in the simulation study. The filtered, 3-D unsteady incompressible Navier-Stokes equations are solved using finite-difference schemes, with a localized dynamic subgrid-scale model to simulate the small-scale motions. For the prediction of the area of the transition, a new, spectral-entropy based method is studied. The proposed method integrates the spectral entropy and energy of the pressure to form a parameter for predicting the location of the transition.

Typical results of computation with Reynolds numbers of 20,000, 50,000 and 100,000 are presented. The results indicate that the transition to turbulence occurred in the shear layer at Reynolds numbers of 50,000 and 100,000. The Λ-vortex structures and the "half mushroom" structures are observed in the transitional flows. The proposed method for predicting the transition is tested. The results of the prediction are compared with the results obtained based on LES and have shown good accuracy.

1 Introduction

This paper studies the numerical simulation of laminar-to-turbulent transition in incompressible flow past a 3-D cavity on solid surface. This research is an extension of our previous studies, which were concerned with incompressible laminar flow past a 3-D open rectangular cavity, at moderate Reynolds numbers in the range from 3,000 to 10,000 [9, 10, 11, 12]. As revealed in the previous studies, as the Reynolds number was increased, the flow fields became highly unsteady and complex, which would strongly affect the boundary layer downstream of the cavity; at some higher Reynolds number, the flow would go into the transitional and turbulent regions. This paper continues the study, focusing on two subjects: 1) numerical simulation of laminar-to-turbulent transition in incompressible flow past a 3-D open shallow rectangular cavity, and 2) prediction of the area of the transition in the shear layer. The prediction and control of transition in shear flows is of high practical relevance. It affects not only skin friction and flow separation, but also heat and mass transfer [1].

Transition and turbulence are unsteady and inherently three dimensional, with both large-scale and small-scale motions. The most straightforward approach to the solution of transition and turbulence is direct numerical simulation (DNS), which directly solves the unsteady Navier-Stokes (NS) equations. This has the advantage that all the scales of turbulence can be resolved, including those that are difficult or impossible to

measure experimentally. But this approach can be computationally expensive, and therefore has largely been limited to simple geometries (e.g. flat plate boundary layers or homogeneous flows) at low Reynolds numbers [5]. To overcome this problem, different methods have been studied which approximate the turbulent flow field as a combination of a mean flow field plus a disturbing flow field. The mean flow field accounts for the large-scale motions, which can be resolved with large grid space; the disturbing flow field simulates the unresolved small-scale motions, which can be produced by an additional turbulence model. Typically, the mean flow field may be obtained by averaging the NS equations over time or space, and the turbulence model may be an empirical model or a subgrid-scale (SGS) model. These correspond to the Reynolds-averaged NS equations (RANS) approach and the large eddy simulation (LES) approach, respectively. More specially, in LES, the spatially averaged NS equations are used to resolve dynamically important large scales, and an SGS model is used to simulate the effect of the unresolved small-scale motions. The SGS model is crude, but in most cases it gives a sufficiently accurate estimate of the effect of the small motions. The LES approach provides a simple yet effective means of simulating the mean-motion properties of a flow throughout the transition region for a reasonably large class of flows. LES can track the temporal evolution of flow disturbances and preserves the frequency content of the free-stream disturbances, which is vital to the transitional process [7].

In this paper, the LES approach is used in the simulation of the transition, with Reynolds numbers equaling 20,000, 50,000 and 100,000, respectively, assuming a laminar Blasius boundary layer inflow condition. In addition, a new, spectral-entropy based method is proposed for predicting the area of laminar-to-turbulent transition in the shear layer of the cavity. The new method locates the transition based on the changes in the pressure spectrum from laminar flow to transitional/turbulent flow. The proposed method may be used for the selection of an appropriate numerical method for the flow structure being modeled. For example, based on the result of the prediction, the laminar NS equations may be used for the laminar flow while LES is used for the transitional and turbulent flow. In comparison to the use of only LES for the whole flow field, this model adaptation method can significantly reduce the computation time and at the same time retain the simulation accuracy.

2 Large Eddy Simulation

It is assumed that the flow is modeled by the 3-D, unsteady, incompressible NS equations. The LES approach includes two parts: 1) the spatially filtered NS equations for large-scale motions, and 2) the SGS model for the small-scale motions that are unresolved in 1). The filtered governing equations are given as follows:

$$\frac{\partial \bar{u}_i}{\partial x_i} = 0 \tag{1}$$

$$\frac{\partial \bar{u}_i}{\partial t} + \bar{u}_j \frac{\partial \bar{u}_i}{\partial x_j} = -\frac{\partial \bar{p}}{\partial x_i} - \frac{\partial \tau_{ij}}{\partial x_j} + \frac{1}{R_e} \frac{\partial^2 \bar{u}_i}{\partial x_j \partial x_j} \tag{2}$$

where, the over-bar denotes the filtered variables corresponding to the large-scale motions,

u_i is the non-dimensional velocity, which is a function of the non-dimensional coordinate x_j and the non-dimensional time t;

$p = p(x_j, t)$ is the non-dimensional pressure;

$R_e = U_\infty L/\nu$ is the Reynolds number, where U_∞ is the free stream velocity, L is the length of the cavity, and ν is the kinematic viscosity;

and τ_{ij} represents the subgrid-scale (SGS) stress tensor, given by

$$\tau_{ij} = \overline{u_i u_j} - \bar{u}_i \bar{u}_j \tag{3}$$

The SGS stress components τ_{ij} correspond to small-scale (i.e. disturbing) motions. These are not resolved in the filtered governing equations. The dynamic SGS viscosity model proposed by Germano [2] is used to simulate τ_{ij}. Further details are given later.

A pressure Poisson equation is employed to couple changes in the velocity field with changes in the pressure field, to satisfy the required continuity condition Equation (1). The filtered version of the pressure Poisson equation can be shown as follows

$$\frac{\partial^2 \bar{p}}{\partial x_i \partial x_i} = \frac{\partial}{\partial x_i}\left(\frac{1}{R_e}\frac{\partial^2 \bar{u_i}}{\partial x_j \partial x_j} - \frac{\partial \tau_{ij}}{\partial x_j} - \bar{u_j}\frac{\partial \bar{u_i}}{\partial x_j}\right) - \frac{\partial}{\partial x_i}\left(\frac{\partial \bar{u_i}}{\partial t}\right) \quad (4)$$

Equations (1), (2) and (4) are solved using the second-order implicit Crank-Nicolson finite difference scheme, which has second-order accuracy in both time and space. At each time step the computation involves the solution of a linear algebraic system with a tri-diagonal matrix. This can be efficiently solved using the alternating direction implicit (ADI) method, which is the method employed in present computation. The SGS stress Equation (3) are modeled by a localized version of the dynamic SGS model, described by Piomelli and Liu [6]. In this model, the model coefficient is calculated by performing a local five-point average for the streamwise and spanwise directions and a three-point average for the wall-normal direction. The total viscosity, including the molecular viscosity and the eddy viscosity, is forced to be non-negative to ensure numerical stability.

Fig. 1 shows the geometric configuration of the rectangular cavity used for computation, where L, W and D represent the length, width and depth of the cavity, respectively. Only a half span of the cavity is shown for clarity. In all the studies, an open shallow cavity is assumed, which has a length-to-depth ratio $L/D = 4$, and a length-to-width ratio $L/W = 1/3$. The Reynolds numbers are chosen based on the length of the cavity. A laminar boundary layer inflow condition is assumed.

The buffer domain technique, proposed by Street and Macarage [8], is used for the outflow boundary condition, in which the governing equations are gradually parabolized in a buffer region which is appended at the end of the computational domain, thus eliminating the necessity of applying the outflow boundary conditions.

Three-dimensional Cartesian non-uniform grids are generated with clustering of nodes near walls and in the shear layer region. These clustered nodes account for greater gradients in velocity and pressure in these regions.

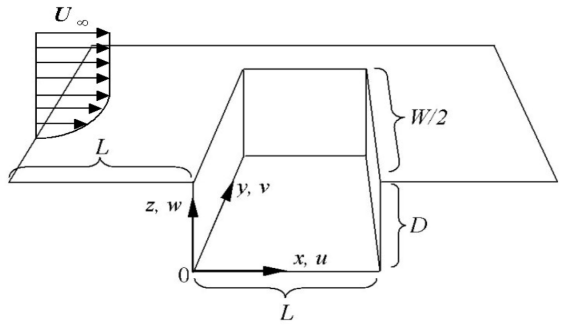

Fig. 1 The rectangular cavity used for computation (only half span is shown for clarity)

3 Typical LES Results of Transition

This section presents selected results of computation of incompressible flow past the 3-D open shallow rectangular cavity, shown in Fig. 1, with $R_e = 20,000$, $50,000$ and $100,000$, respectively. The thickness of the laminar boundary layer inflow is $\delta = 0.05$ for $R_e = 20,000$, $\delta = 0.035$ for $R_e = 50,000$, and $\delta = 0.025$ for $R_e = 100,000$, which correspond to an inflow distance of approximately $2L$.

Fig. 2 shows the contours of the streamwise velocity on the $x-y$ plane at $z = 0.26$ (with $(z-D)/\delta^* = 0.3$), away from the bottom of the cavity, for $R_e = 20,000$, $50,000$ and $100,000$, respectively. At $Re = 20,000$, small vortices can be seen around the side walls of the cavity. Although the Kelvin-Helmholtz (K-H) instability can be observed in the shear layer over the cavity, the flow should remain laminar due to the absence of the Λ-vortices [3]. At $Re = 50,000$, the Λ-vortices are apparent in the shear layer, as structures at about 60° to the main flow direction caused by curving and stretching of the K-H

vortices into the cavity. They have already become strong enough and gone into the stage of transition. The Λ-vortices are followed immediately by the laminar breakdown and transition into turbulence. At $Re = 100,000$, the occurrence of the Λ-vortices, and hence the transition, is moved upstream closer to the front wall of the cavity. For $Re = 50,000$ and $100,000$, the 2-D Tollmien-Schlichting (TS) waves are observed in the boundary layer before the cavity, as shown in Figure 2 (b) and (c). Above the cavity, the laminar flow is approaching breakdown and is in transition; three-dimensional disturbances are obtained in the shear layer. At the downstream of the cavity, the flow becomes turbulent.

Fig. 3 shows the instantaneous velocity vectors on the $x-z$ plane at $y = 0$, for $R_e = 20,000$, $50,000$ and $100,000$, respectively. In all the three cases, a primary vortex is found at the downstream end of the cavity, and a secondary vortex is found upstream. In addition, some tertiary vortices can be found upstream of the cavity below the shear layer. All the three cases indicate the K-H instability in the shear layer over the cavity. As shown in Fig. 3, as the R_e increases, the K-H instability becomes stronger, as indicated by the increasingly violent shear layer oscillations, and the tertiary vortices become larger and develop closer to the front wall of the cavity. It can be noticed that, as the R_e increases, the occurrence of the K-H instability is located away from the rear wall of the cavity towards upstream.

Fig. 4 presents the contours of the spanwise vorticity corresponding to Fig. 3, showing the variations of the boundary layer and shear layer during the transition. At $R_e = 20,000$, the shear layer directly impinges on the downstream boundary of the cavity, indicating that the flow may have not undergone transition to turbulence. At $Re = 50,000$, a vortex is shed from the shear layer in the middle of the cavity, a detached high shear layer appears above the cavity, and multiple shear layer roll-ups occur, indicating that the flow reaches laminar breakdown and is in transition to turbulence. A similar transitional vortical phenomena can be observed for the flow at $Re = 100,000$. In comparison to $Re = 50,000$, at $Re = 100,000$, the occurrence of the transition is moved upstream closer to the front wall of the cavity, due to an earlier shedding of the vortex from the shear layer.

Fig 5 shows the contours of the streamwise velocity on the $y-z$ plane at $x = 2.5$, located at the downstream of the cavity. As shown, for $R_e = 50,000$ and $100,000$, the distortions of the mean velocity are so strong that the so-called "half mushroom" structures are observable. This structure (or vortex rollover state) is accompanied by the double inflection points in the wall-normal profiles of the streamwise velocity.

4 Prediction of the Location of Transition - Theory

In this paper, a new approach for locating the area of laminar-to-turbulent transition is proposed. This approach locates the transition based on the changes in the pressure spectrum from laminar flow to transitional/turbulent flow. To illustrate this approach, Figure 6 shows the power spectrum of the pressure fluctuation at different x locations, i.e. before, within, and after the cavity, for $R_e = 50,000$. As shown in the figure, before the cavity ($x < 0$), there is almost no random disturbance in the pressure, indicating that the flow is laminar. Fluctuations in the pressure are seen within the cavity ($0 \leq x \leq 1$), which are slow before the transition and so the spectrum is concentrated in the low-frequency region. After the transition, at the downstream of the cavity ($x > 1$), the pressure becomes violent, so multiple spectral peaks are seen across a wider frequency range. In general, it may be assumed that the pressure of laminar flow exhibits a slow-varying and often pseudo-periodic characteristic, and therefore its power spectrum is concentrated in the low-frequency region with a small bandwidth; when the flow goes into transition and into turbulence, the pressure becomes more erratic, showing the characteristic of a white noise, and therefore its power spectrum will be distributed in a much wider frequency range. Therefore, the difference in the spread or bandwidth of the power spectrum of the pressure fluctuation can

be exploited for separating the laminar flow and transitional/turbulent flow. To achieve, the entropy defined in information theory can be used to quantify this difference.

In information theory [4], entropy is a measure of the degree of uncertainty on the value of a random variable. Assume that a random variable can take any of the N values $\upsilon_1, \upsilon_2, \cdots, \upsilon_N$, with a probability $q(\upsilon_n)$ for taking value υ_n, satisfying the constraints $q(\upsilon_n) > 0$ and $\sum_{n=1}^{N} q(\upsilon_n) = 1$. Then the entropy is defined as

$$H = -\sum_{n=1}^{N} q(\upsilon_n) \ln q(\upsilon_n) \tag{5}$$

It can be shown that when all $q(\upsilon_n)$'s are equal, i.e., when the random variable takes each of the N values with equal probability and hence its value is most uncertain, H reaches the maximum [4]. In the maximum-entropy situation, the probability distribution $q(\upsilon_n)$ spreads over the entire value set $\upsilon_1, \upsilon_2, \cdots, \upsilon_N$ and the shape of the distribution is completely flat. As such, the value of entropy reflects the spread and flatness of a distribution. To apply this to the power spectral distribution, for a given power spectrum $s(f_n)$, where $s(f_n)$ represents the power at the frequency component f_n, $n = 1, 2, \cdots, N$, we can obtain a probability distribution $q(f_n)$ based on $s(f_n)$ by normalizing the $s(f_n)$, i.e.

$$q(f_n) = \frac{s(f_n)}{\sum_{k=1}^{N} s(f_k)} \tag{6}$$

Since a laminar flow typically has a narrow-band power spectrum that is neither flat nor widely stretched over the entire frequency domain, its distribution $q(f_n)$ should have a low entropy. Since a transitional/turbulent flow has a more widely spread and hence more flat power spectrum than the laminar flow, its distribution $q(f_n)$ should have a higher entropy. Thus, a significant rise in the value of the entropy can be an indication of the occurrence of a laminar-to-turbulent transition.

When the pressure fluctuation is dominated by random numerical instability, a high entropy may also result. This problem can be overcome by ignoring the pressure fluctuation with a small energy. This leads to a parameter, the product of the entropy and energy for predicting the transition:

$$\alpha = H \cdot E \tag{7}$$

where E is the energy of the pressure fluctuation.

In the simulation, the parameter α is calculated for each time t and each location (x, y, z). The required power spectrum and energy of the pressure fluctuation for each location at time t are calculated based on M pressure samples at that location observed at and before t ($M = 100$ in the present computation). The power spectrum is derived using Fast Fourier Transformation (FFT) and the energy is obtained as the sum of the squared samples.

5 Prediction of the Location of Transition - Typical Results

The above method has been applied to the location of laminar-to-turbulent transition, for the problem of incompressible flow past a 3-D rectangular cavity described in Section 3. As an example, Figs. 7, 8 and 9 show the values of the entropy H, energy E and the parameter α, for $R_e = 20,000$, $50,000$ and $100,000$, respectively, as a function of x at $t = 20$, $y = 0$ and $z = 0.26$. Fig. 7 indicates that the entropy increases with R_e, which correctly captures the flow instability. In particular, Fig. 7 (b) and (c), for $R_e = 50,000$ and $100,000$ respectively, show a sharp increase in entropy in the shear layer at $x \simeq 0.5$ and $x \simeq 0.1$, where the respective transition takes place. However, before the cavity ($x < 0$) where the flow is laminar, the entropy is not small because of the random numerical instability. Fig. 8 indicates that the energy of the pressure fluctuation caused by the numerical instability is usually extremely small. Therefore, the effect of the numerical instability can be effectively removed by multiplying the entropy shown in Fig. 7 by the corresponding energy shown in Fig. 8. This leads to the parameter α shown in Fig. 9, which clearly indicates, by a sharp increase in the α value, that a transition may have occurred at $x \simeq 0.5$ for

$R_e = 50,000$, and at $x \simeq 0.1$ for $R_e = 100,000$. The occurrence of a transition for $R_e = 20,000$ may be ruled out because of the small α values.

A further example, showing the parameter α as a function of x and y , at $t = 20$ and $z = 0.26$, is given in Fig. 10. The new feature has clearly indicated the transition/turbulence areas in both x and y directions, at the given time and the horizontal plane. These results of location have been compared with the results obtained based on LES described in Section 3 and have shown good accuracy.

References

[1] Bippes H. Basic experiments on transition in three-dimensional boundary layer dominated by crossflow instability. *Progress in Aerospace Science*, Vol. 35, pp 363–412, 1999.

[2] Germano M, Piomelli U, Moin P, and Cabot W. H. A dynamic subgrid-scale eddy viscosity model. *Phys. Fluids A*, Vol. 3, pp 1760–1765, 1991.

[3] Huai X, Joslin R. D, and Piomelli U. Large-eddy simulation of transition to turbulent in boundary layers. *Theoretical and Computational Fluid Dynamics*, Vol. 9, No 2, pp 149–163, 1997.

[4] Kullback S. *Information Theory and Statistics.* 1st edition, New York: Dover, 1969.

[5] Piomelli U. Large-eddy simulation: achievements and challenges. *Progress in Aerospace Science*, Vol. 33, pp 335–362, 1999.

[6] Piomelli U and Liu J. Large eddy simulation of rotating channel flow using a localized dynamic model. *Phys. Fluids*, Vol. 7, pp 839–848, 1995.

[7] Singer B. A. Modeling the transition region. *NASA CR-4492*, 1993.

[8] Street C. L and Macaraeg M. G. Spectral multi-domain for large-scale fluid dynamics simulations. *Int. J. Applied Num. Meth.*, Vol. 6, pp 123–139, 1989.

[9] Yao H, Cooper R. K, and Raghannathan S. Computation of incompressible flow over three-dimensional cavities. *Proc Advances in Fluid Mechanics (AFM'2000)*, Vol. III, pp 125–133, Montreal, Canada, 2000.

[10] Yao H, Cooper R. K, and Raghannathan S. Incompressible laminar flow over a three-dimensional rectangular cavity. *International Journal of Thermal and Fluid Sciences*, Vol. 9, No 3, pp 199–204, 2000.

[11] Yao H, Cooper R. K, and Raghannathan S. Numerical simulation of incompressible laminar flow over 3-d cavity. *Proc Computational Fluid Dynamics 2000 (ICCFD'2000)*, pp 253–258, Kyoto, Japan, 2000.

[12] Yao H, Cooper R. K, and Raghannathan S. Simulation of three-dimensional incompressible cavity flows. *Proc 22nd International Congress of Aeronautical Sciences (ICAS'2000)*, pp pp. 296.1–296.8, Harrorgate, UK, 2000.

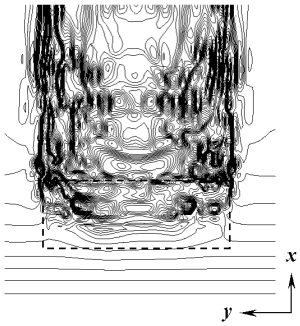

(a) $Re = 20,000$

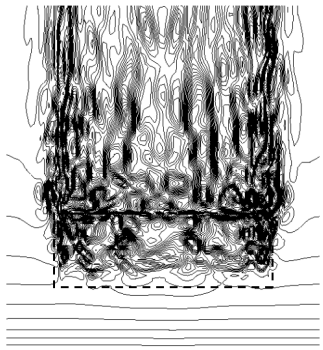

(b) $Re = 50,000$

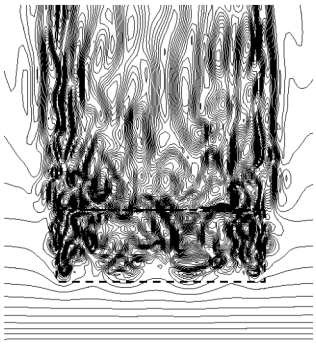

(c) $Re = 100,000$

Fig. 2 : Contours of the streamwise velocity on the $x-y$ plane at $z = 0.26$, $t = 20$

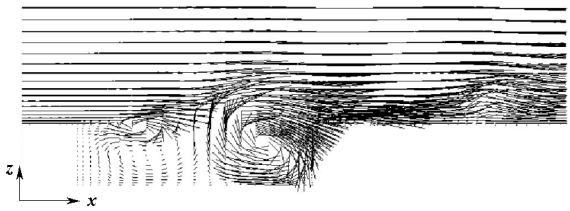

(a) $Re = 20,000$

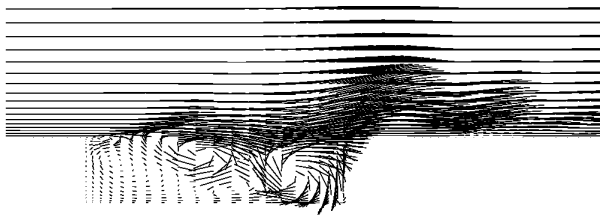

(b)$Re = 50,000$

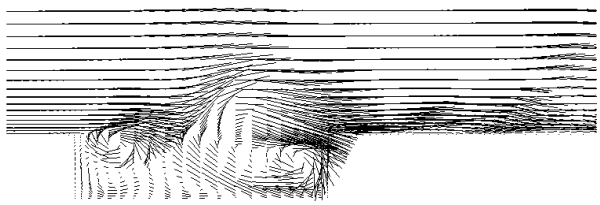

(c) $Re = 100,000$

Fig. 3 Instantaneous velocity vectors on the $x-z$ plane at $y = 0$, $t = 20$

(a) $Re = 20,000$

(b) $Re = 50,000$

(c) $Re = 100,000$

Fig. 4 : Contours of the spanwise vorticity on the $x-z$ plane at $y = 0$, $t = 20$

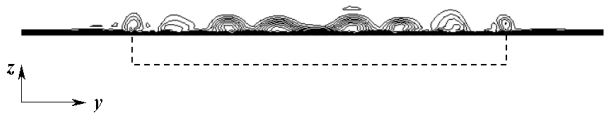

(a) $Re = 20,000$

(b) $Re = 50,000$

(c) $Re = 100,000$

Fig. 5 : Contours of the streamwise velocity on the $y-z$ plane at $x = 2.5$, $t = 20$

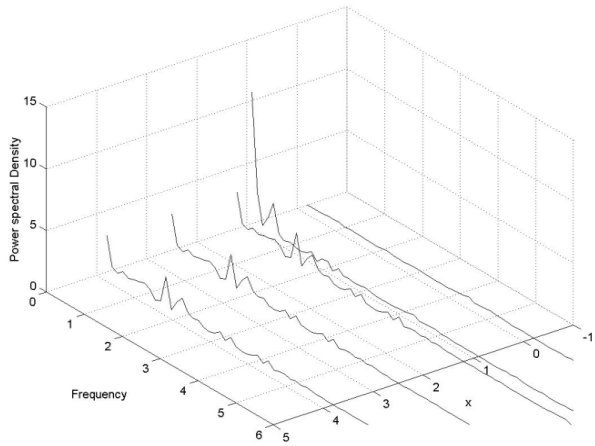

Fig. 6 : Power spectral densities of the pressure fluctuation at different streamwise locations before the cavity ($x < 0$), in the cavity ($0 \leq x \leq 1$) and after the cavity ($x > 1$), for Re=50,000

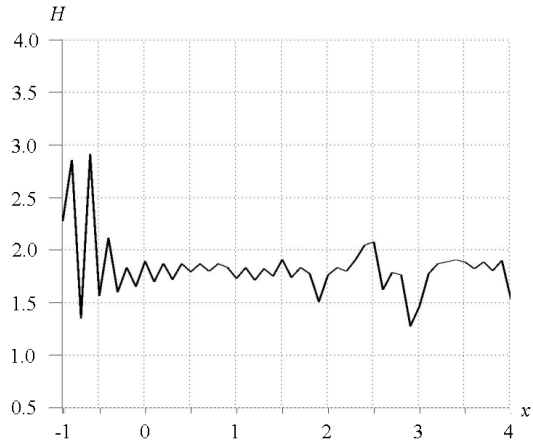

(a) $Re = 20,000$

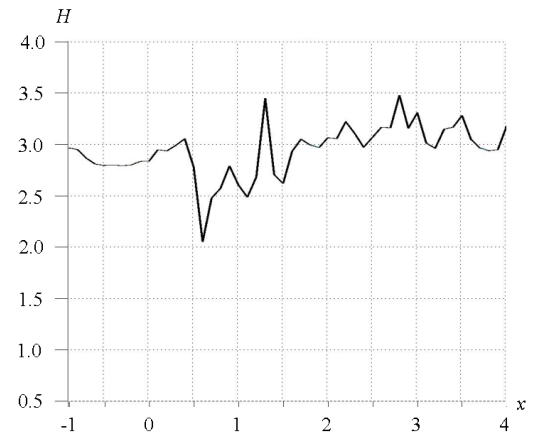

(b) $Re = 50,000$

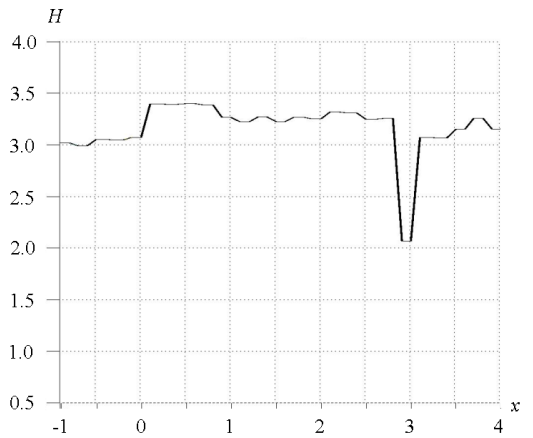

(c) $Re = 100,000$

Fig. 7 : The values of entropy H as a function of x at $y = 0$, $z = 0.26$, $t = 20$

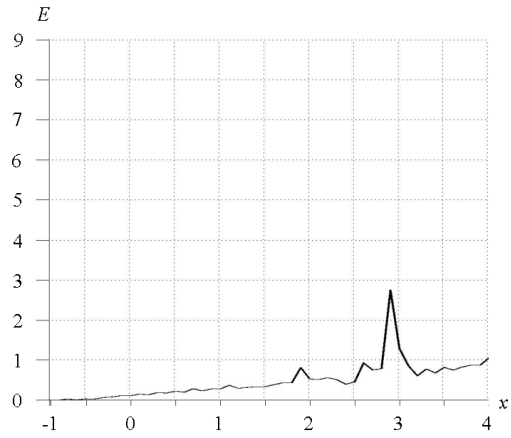

(a) $Re = 20,000$

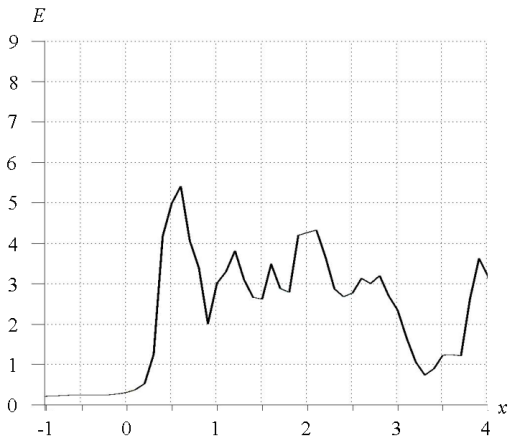

(b) $Re = 50,000$

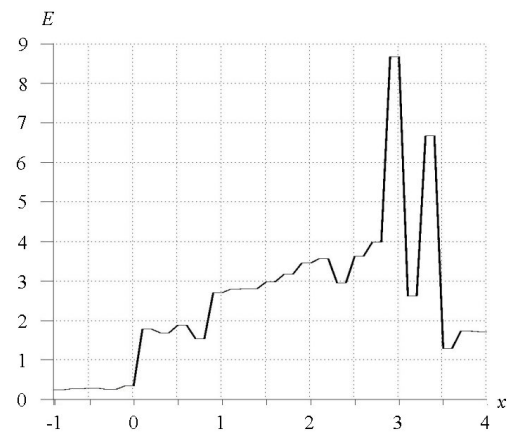

(c) $Re = 100,000$

Fig. 8 : The values of energy E as a function of x at $y = 0$, $z = 0.26$, $t = 20$

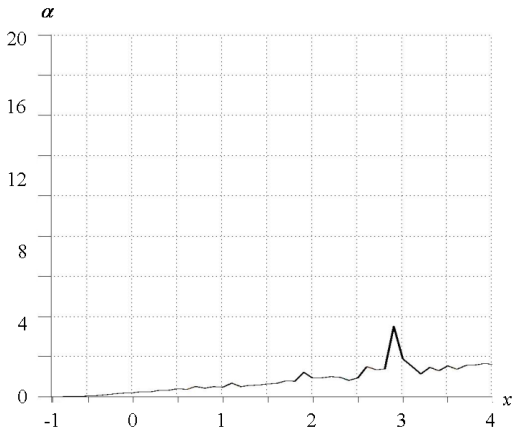

(a) $Re = 20,000$

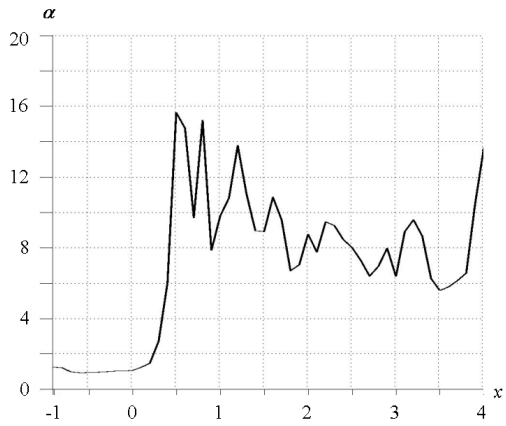

(b) $Re = 50,000$

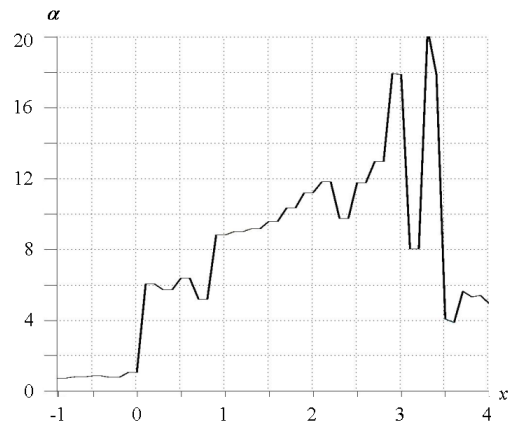

(c) $Re = 100,000$

Fig. 9 : The values of the parameter α as a function of x at $y = 0$, $z = 0.26$, $t = 20$

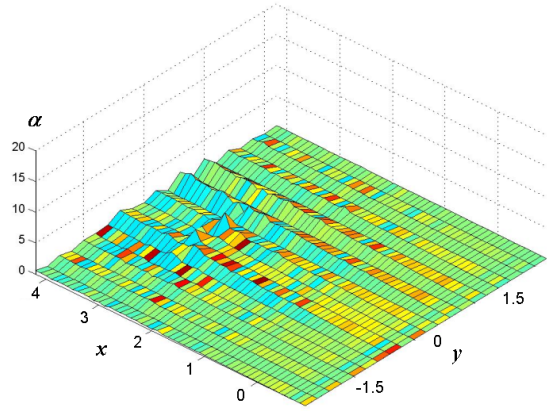

(a) $Re = 20,000$

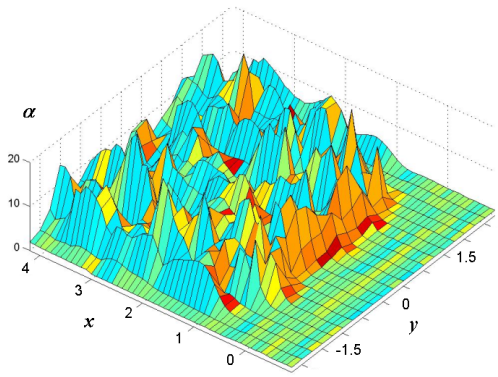

(b) $Re = 50,000$

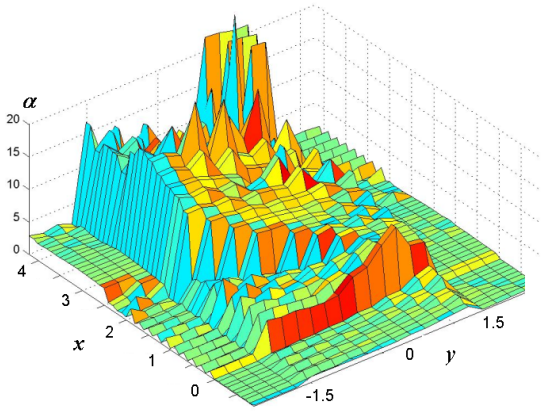

(c) $Re = 100,000$

Fig. 10 : The values of the parameter α as a function of x and y at $z = 0.26$, $t = 20$